LJMU Research Online

Eslami Majd, A and Ekere, NN

 Crack initiation and growth in PV module interconnection

http://researchonline.ljmu.ac.uk/id/eprint/15724/

Article

For more information please contact researchonline@ljmu.ac.uk

1 **Crack Initiation and Growth in PV Module Interconnection**

2 Alireza Eslami Majd[a*] and Nduka Nnamdi Ekere[a]
3 [a]School of Engineering, Faculty of Science and Engineering, University of Wolverhampton, UK

4

6 **Abstract**
7   As the cost of PV (photovoltaic) solar panels drops, it is widely expected that solar energy will
8 become the cheapest source of electricity in many parts of the world over the next two decades. To
9 ensure that PV solar modules have a long service life and can meet the PV manufacturer's warranty,
10 the PV modules need to have high reliability. Solar PV module manufacturers typically provide two
11 warranties: a performance warranty which guarantees 90% of original power output after 10 years and
12 80% of original output of at 25 years; and an equipment warranty which guarantees their PV module
13 will have a minimum of 10-12 years operation before failure. A critical part of the solar PV module
14 assembly is the ribbon interconnection between the solar cells (i.e. the solder joint interconnections),
15 and failure of the ribbon interconnection can adversely affect the performance and reliability of whole
16 PV module. Ribbon interconnection failures have been linked to the thermal cracks which are initiated
17 in the solder joint material during the high temperature ribbon interconnection manufacturing process;
18 and then the crack propagation and growth associated with the thermal cycling of the ribbon
19 interconnections under higher than ambient temperature PV module operating conditions. This paper
20 reports on the study of high temperature crack initiation and propagation in different PV Module
21 interconnection configurations by using XFEM in ABAQUS software. It concerns a necessary, urgent
22 and fundamental revision of the manufacturing process that lies at the heart of PV module ribbon
23 interconnection manufacture.

24

---

* Corresponding author
  E-mail addresses: a.e.majd@wlv.ac.uk

1. Introduction

With massive investments in renewable energy in recent years; renewable energy is establishing a strong foothold in the global energy system at a faster rate than any other fuel source in history; and for this reason renewable energy is expected to become the world's main source of power within two decades. Indeed, the International Energy Agency (IEA) 2014 Technology Roadmaps for Solar Photovoltaic Energy and for Solar Thermal Electricity concluded that solar energy could surpass fossil fuels, wind and hydro by 2050 to be the world's largest energy source. This is because generating electricity from solar energy, an abundant and renewable source, using photovoltaic (PV) systems has become very widespread. This increase in the use of photovoltaic (PV) solar systems for generating electricity has been driven by subsidy programs and economic incentives for investments by several governments. Due to the increased economic incentives, the worldwide growth of solar PV has been close to exponential between 1992 and 2018; thereby helping solar PV technology to evolve from a niche market of small scale applications to a mainstream electricity source. This growth in PV solar is set to continue, according to the IEA's latest 5-year forecast, renewable power capacity is set to expand by 50% between 2019 and 2024, led by solar PV (IEA, 2019).

The solar PV cells (panels) technology has been used in several applications over the years – for example, they have been utilised successfully as an energy source on rooftops, spacecraft, handheld calculators and other wearable electronic devices. The motivation for this study is to investigate novel PV Module interconnection configurations which can improve the PV module power output by increasing the incidence of light onto the PV solar module also lead to increased ribbon interconnection reliability.

1.1 Reliability of PV modules

Unlike other electrical equipment, PV modules are unique in that they carry very long-term performance warranties of 20 - 25 years (indeed, very few types of electrical equipment have such long warranties). For this reason, improving the reliability of PV modules remains a major R&D challenge; as reliability is neither defined nor covered by the existing quality certification standards such as the IEC 61215 (IEC International Electro technical Commission); thus the design qualification to those standards does not imply the PV module's reliability. This lack of reliability standards is partially due to the fact that PV solar module technology is still in its infancy (with most PV installations yet to reach their 20 to 25 year lifetime as per warranty), and thus there is very little or no statistical data available on PV module field failure (Ferrara & Philipp, 2012), (Ishii & Atsushi, 2017). This study concerns a necessary, urgent and fundamental revision of the soldering process that lies at the heart of PV module ribbon interconnection manufacture. Through a new methodology, it addresses the modelling of the impact of different PV Module interconnection configurations on the crack initiation temperatures and crack growth rates for improved PV Module interconnection reliability.

62   The ribbon interconnection of the PV solar module is critically important in component. The ribbon

63   interconnection is soldered directly onto silicon crystals to interconnect solar cells in the PV module

64   and it plays an important role in determining cell efficiency, as it serves to carry the current generated

65   in the solar cells to the PV busbar. The ribbon solder interconnection has been reported as the most

66   susceptible part of the PV module system, and hence the dominant factor in PV module degradation

67   and responsible for over 40% of recorded field PV module failures (Hermann, 2010). Also in their

68   validation of the PV Life model using 3 million module-years of live field data, Hasselbrink, et al.

69   comprehensively reviewed the customer fleet returns sheets focussing on the reasons for returns due to

70   failure over an average deployment period of 5 years; and they found that circa 66% of the returns were

71   due to solder interconnection failures, whilst encapsulate and back-sheet failures accounted for circa

72   22% of returns (Hasselbrink, et al., 2013).

73   There are several works on analysis of crack in the Silicon material of PV module. For example, in

74   Silicon layers exposed to thermal cycling and to mechanical loading, cracks were observed mainly at

75   the beginning and the end of the busbars which the cracks grow along the busbars (M. Sander, et al.,

76   2011). However, there are no enough works on the crack initiation and growth in the interconnection

77   material of PV modules to improve the reliability. For this reason, the focus of the recent PV module

78   reliability studies has been on the ribbon interconnection design and failure. These include some

79   experimental studies focussed on the investigation of the failure mechanism of the ribbon

80   interconnection and this shows that the solder coating on the ribbon interconnection is the most common

81   source of failure. The ribbon interconnection failure is mostly linked to crack initiation and propagation

82   in the solder joints material which exhibits brittle mechanical behaviour. The nucleated crack in the

83   solder joint can lead to hot spots resulting from high contact resistance at the ribbon and the cell

84   interface and then potentially results in DC arc (Itoh, et al., 2014). In addition, these hot spots can also

85   lead to the degradation of the encapsulation and partial shading cell effect; consequently this problem

86   impacts on the parameters of performance and reduces power outputs and the efficiency of the PV

87   module (Bidram, et al., 2012) and (Pareek, et al., 2017).

88   Few of the reported analytical/numerical studies on the failure of the PV module interconnection

89   (solder joint) have considered the modelling of nonlinearities in their investigation failure and most

90   studies have only assumed linearity and early elastic states. (Wang, et al., 2016). Equally, in their

91   consideration of the influence of the coefficient of thermal expansion (CTE) of the PV module materials

92   on the stress level, most studies have assumed linear and temperature independent behaviour. The focus

93   of this study is to incorporate nonlinearities and temperature dependence in the investigation of the

94   impact of ribbon interconnection design on the failure and reliability of PV solar modules.

95   **1.2 Problem Context**

96   In spite of the best efforts of manufacturers to minimise and control thermomechanical stress effects

97   on the PV module, the high temperature process can lead to micro-cracks in the ribbon interconnection

98   solder joint material and the cells, which can lead to crack nucleation and propagation and subsequent

99   interconnection failure. This can be explained by the fact that during the hot temperature manufacturing

100   process, the coefficient of thermal expansion (CTE) mismatch (between interconnecting materials)

101   results in high levels of stress and strain; and this accumulation of strain energy is responsible for the

102   initiation of micro-cracks in the solder joint materials.

103   Experimental studies have shown that with high temperature cycling of PV modules (such as those

104   experienced by PV modules during in high temperature climates), the micro-cracks initiated in the

105   solder joint material can grow and propagate through the connecting layer and ultimately lead to PV

106   module failure. This is particularly true with lead-free solder joint materials (which is now the preferred

107   environment-friendly joining material), as they have higher probability of developing micro-cracks due

108   to their lower fracture strength and higher thermo-mechanical stress levels when compared to tin-lead

109   solder alloys (Pander, et al., 2014).

110   1.3 Solder Fracture

111   A number of previous studies have reported on the fracture mechanics and the effect of solder joints

112   geometry on the reliability of electronics assembly board interconnections subjected to thermo-cycling

113   loads. These include the development of an empirical equation for predicting the thermal-fatigue life of

114   solder bumps using the measured crack growth rate at the crack tip (H. Lau, et al., 2001); the predict

115   the effect of solder joint geometry on the reliability of Ball Grid Array (BGA) solder joints on flexible

116   and rigid PCBs subjected to thermo-cyclic loading (Lau, et al., 2014) ; the investigation of the impact

117   of Inter Metallic Component (IMC) on the reliability of lead-free solder joints at elevated temperature

118   operation (H. Amalu & N.N. Ekere, 2011) and modelling evaluation of Garofalo-Arrhenius creep

119   relation for lead-free solder joints in surface mount electronic component assemblies (H. Amalu & N.N.

120   Ekere, 2016). The results of these previous studies show that the thermal fracture mechanism of a solder

121   joint interconnection can generally be sub-divided into two distinct modes. Firstly, the fractures that

122   occur inside the solder joint due to solder grain size growth and the corresponding decrease in bonding

123   strength during thermal cycling, which then leads to crack propagation at the interface of large grain.

124   Secondly, the fractures that occur at the interface of solder with interconnection material (that is within

125   the Inter Metallic Component (IMC) layer formation); for example Cu_5Sn_6 and Ag_3Sn which is formed

126   through the dissolution of the Ag/Cu materials in the solder (Itoh, et al., 2014). A recent study on the

127   investigation of the effect of non-homogenous solder coating on the micro-crack initiation temperature

128   in the round wire Multi-Busbars of the PV solar module showed that the crack nucleates at the edge of

129   the IMC layer; and the interface between the solder joint and silver pad (Eslami Majd & Ekere, 2019).

130   Another simulation study shows that higher strain rates and thicker IMC's results in IMC-interface

131   brittle fracture or IMC-controlled fracture; whilst lower strain rates and smaller IMC thickness leads to

132   solder-internal fracture or solder-controlled fracture (Fei, et al., 2012). Results from a study on the

133   analysis of experimental samples have shown that the Ag to solder crack in IMC region is more

134 prevalent than the Cu to solder region crack (Jeong, et al., 2012), whilst the studies by Li, et al showed
135 that fractures and the straight crack propagation path tends to be located on the component side of the
136 solder interconnections (beneath die edge) (Li, et al., 2012); and that the tensile and the shear strength
137 of IMC layers decrease with increase in the IMC layer thickness (Zhong, et al., 2010).

138   In this Study, we investigate the micro-crack initiation and growth in the lead free solder joint
139 material of the conventional PV Module ribbon interconnections during high temperature
140 manufacturing process. The results of the study will be beneficial for researchers in predicting the
141 propagation paths for existing micro-cracks during the thermal fatigue cycling under in-service PV
142 module operating conditions; and hence for the predicting of PV Module interconnection reliability.
143 The XFEM in ABAQUS Software was used for this study as it enables the accurate solution of boundary
144 value problems with discontinuities and singularities freely located within elements of the mesh (Fries,
145 2018). The XFEM facilitates stress intensity factor computations even on relatively coarse meshes, and
146 further-more, no re-meshing is required for crack growth simulations.

2. Finite Element Modelling and Simulation

148 The Extended Finite Element Method (XFEM) feature of the ABAQUS 2019 is employed for
149 determining the critical temperature for micro-crack initiation and growth in PV module ribbon
150 interconnections. The XFEM is based on the generalized finite element method (GFEM) and the
151 partition of unity method (PUM), and this numerical technique extends conventional finite element
152 method and allows local enrichment discontinuous functions to be combined with the numerical
153 approximation. Unlike ordinary FE methods, with the XFEM method there is no need to define the
154 crack location beforehand. In effect, the XFEM models a crack within an enriched element by adding
155 degrees of freedom in elements with special displacement functions. This means that while XFEM is
156 generating discontinuous fields along a crack and around its tip, there is no need for modelling the
157 geometry of crack and re-meshing in the simulation (ABAQUS, 2017). The detailed formulas and
158 further information for XFEM can be found in (Mohammadi, 2008) and (Moës, et al., 1999).

159

2.1 Structure and Geometry of Models

161   Figure 1 shows the schematic view of the assembly of the ribbon interconnections between solar
162 cells in the PV module assembled by back to front connection method. The PV solar module is typically
163 built up of different materials, including: silicon as the semiconductor material, EVA (ethyl vinyl
164 acetate) which serves as encapsulate materials to protect solar cells, aluminium sheet to envelop the
165 backside of the silicon, the pasted silver pads and fingers to receive the electrical current, Tedlar
166 (Polyvinyl Fluoride) as a back sheet to cover the bottom, glass as front cover and the copper wire coated
167 by solder materials to collect the electrical current from the individual cell.

168   In this study the thickness of aluminium, silicon cell, EVA, glass and Tedlar layers used for the FE

169   models are assumed to be 25µm, 200µm, 460µm, 3mm and 190µm, respectively. The thickness of other

170   component parts such as silver pad, copper, solder used and the ribbon interconnection width have been

171   varied to investigate the effect of ribbon interconnection geometry and design on the crack initiation

172   and propagation parameters.
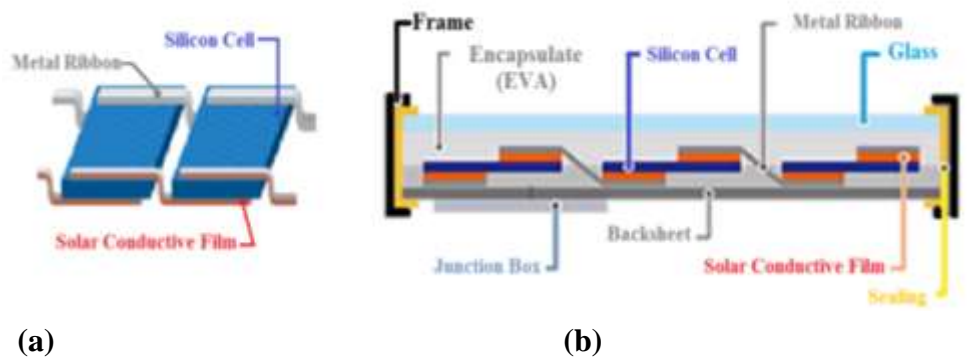
173

174   **(a)**   **(b)**

175   Figure 1 Ribbon interconnections assembly between cells in the PV Module (a) Side view of cross section of PV
176   modules included Materials (b)

177   Also, in this study to take account of the high ratio of the ribbon interconnection length to the other

178   dimensions of model, the 2D plane-strain elements (CPE3[2] and CPE4[3]) have been used to increase the

179   computational solution speed. The symmetry boundary condition is applied to the mid-point of the

180   ribbon interconnection section and bottom-end of the Tedlar material is closed. Figure 2, presents the

181   schematic view of ribbon interconnection FE model; showing the boundary conditions, the arrangement

182   of component materials and the meshing style (**Note**: the fine meshing technique is used for crack area

183   in the solder joint material).

---

[2] A 3-node linear plane strain triangle
[3] A 4-node bilinear plane strain quadrilateral
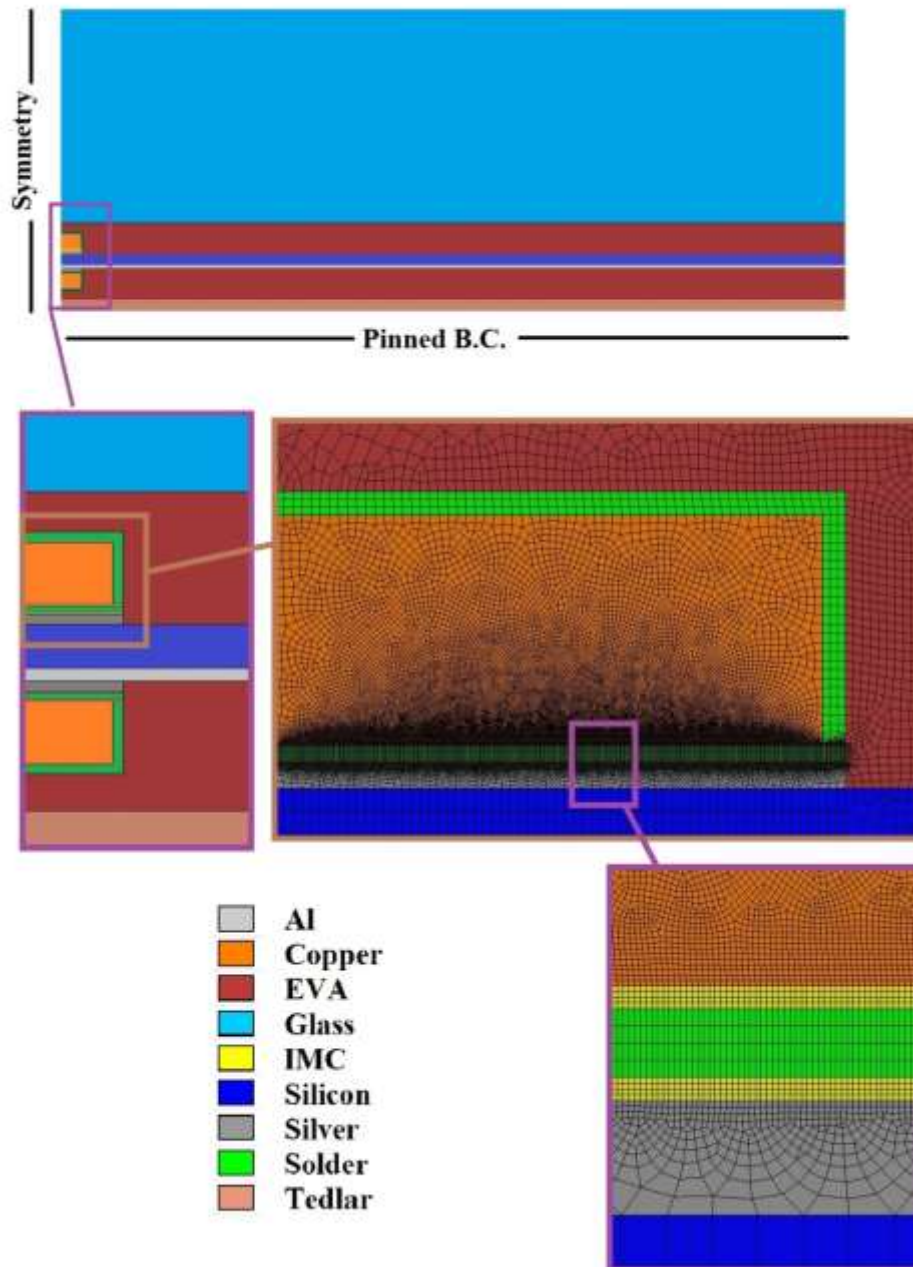
184
Figure 2 Schematic view of 2D simulation of ribbon interconnection with showing boundary conditions, mesh styles and arrangement of materials

2.2 Load Condition

In this study, the thermal load is applied uniformly to the model as the temperature of all components of the PV module is assumed homogenous and the temperature is applied linearly by increments of 15^0C per minute.

2.3 Material Properties

The mechanical properties of the material used in the simulation are presented in Table 1. For metallic materials, plastic behaviour has been assumed and linear elastic behaviour is assumed for the IMC layer (due to its brittleness). Based on cohesive traction-separation law method, the maximum nominal stress (MAXS) in the shear and tensile directions are considered as the controlling parameters for the damage initiation in the IMC layers. This means that the damage (crack) is initiated when these components exceed the defined limits, and then the initiated crack will be evaluated as a function of the fracture energy. For a more realistic simulation, we investigate the effect of temperature dependence of important material properties such as coefficient of thermal expansion of silicon and metallic materials and the Young's Modulus and plastic behaviour of the solder joint material (see Table 2).

Table 1 Mechanical Properties of Material used in the FEM simulation of ribbon interconnection

Parameter (unit)	Material								
	IMC (Deng, et al., 2005) & (Zhong et al., 2010)	Solder Joint	Silver (AZoM, 2001)	Copper (Jing, et al., 2015)	EVA (Cambridge University Engineering Department, 2003)	Silicon (Owen-Bellini, et al., 2015)	Aluminium (AZoM, 2005)	Tedlar (DuPont™, 2014)	Glass (Tippabhotla, et al., 2017)
Elastic Modules (GPa)	110	See Table 2	69	121	11	130	68.3	2.138	73.0
Poisson's Ratio (-)	0.3	0.35	0.365	0.34	0.499	0.28	0.34	0.4	0.235
Yield Stress (MPa)	-	-	43	121	12	170	85	41	-
Shear Strength (MPa)	27.6-1.95*H_{IMC}	30	120	248	16	-	60	-	-
Tensile Strength (MPa)	65	78	120	248	16	-	100	-	-
Fracture Toughness (MPa.m^0.5)	1.4	7	40	30	-	0.83	22	-	-
Thermal Expansion Coefficient (ppm/k)	See Table 2	See Table 2	See Table 2	See Table 2	270	See Table 2	See Table 2	78	8.0
Plastic Stress-Strain Curve (MPa)	-	See Table 2	43@0.001 120@0.04	121@0.001 186@0.004 217@0.01 234@0.02 248@0.04	-	-	85@0.00 100@0.12	41@0.00 55@0.9	-

Table 2 Temperature dependent properties of interconnection materials

Temp. (c)	CTE for Copper (ppm/k) (Taulaukian, et al., 1975) (Interpolated)	CTE for Silicon (ppm/k) (Sasi Kumar, et al., 2017) (Interpolated)	CTE for Silver (ppm/k) ((Taulaukian, et al., 1975) (Interpolated)	CTE for Aluminium (ppm/k) (Taulaukian, et al., 1975) (Interpolated)	CTE for IMC (ppm/k) (Jiang, et al., 1997) (Interpolated)	CTE for Solder (ppm/k) (21.3+0.017T) (Li, el al., 2012)	Solder Young's Modulus (GPa) (49-0.07T) (Li et al., 2012)	Plastic Stress for Solder (MPa) (at 0.0, 0.065 Plastic Strain) (Siviour, et al., 2005) (Interpolated)
0	16.22	2.35	18.67	22.50	17.7	21.3	49	71, 145
30	16.60	2.63	18.98	23.29	18	21.81	46.9	52, 131
60	16.91	2.87	19.20	23.85	18.3	22.32	44.8	16, 110
90	17.22	3.04	19.42	24.41	18.6	22.83	42.7	-
120	17.53	3.20	19.65	24.97	19	23.34	40.6	-
150	17.76	3.36	19.91	25.40	19.8	23.85	38.5	-

3. Results and Discussion

204 This section presents the results and analysis of the simulation modelling for different PV module

205 ribbon interconnection configurations and design parameters. The crack location, the crack initiation

206 temperature and crack propagation rate are determined for each state. Our results show that the crack

207 initiation temperature and crack propagation rate are quite dependent on the dimensions of ribbon

208 interconnection. The effect of different PV module ribbon interconnection configurations and design

209 parameters the crack initiation temperature and crack propagation rate are presented in the sub-sections

210 below.

3.1 Effect of Changing Solder and IMC Thickness

212 The results from our FEM simulation showed that increasing the solder coating thickness leads to

213 a decrease in the crack initiation temperature (circa linear relationship); and this reduction in crack

214 initiation temperature is more pronounced for thicker IMCs (see Figure 3). This can be explained by

215 the higher stress levels in the solder joint material and the strain accumulated in the IMC layer which

216 results in crack initiation at lower temperatures. This result is not in line with the expectation that a

217 thicker solder coating will result in higher interconnection reliability (a stronger solder joint that will

218 be more resilient to premature failures).

219 Figure 4 presents a plot of the effect of solder coating and IMC thickness on the crack growth rate.

220 The results show that the crack growth rate is almost constant for the solder coating thickness under

221 50μm, but further increases in solder coating thickness beyond the 50μm limit leads to a big jump in

222 the crack growth rate. Figure 4 also show that the crack growth rate is much lower in the thicker IMC

223 layers compared to thinner IMC layers.

224 As can be seen in Figure 5, for all the simulation results presented in Figure 3, the location for the

225 crack nucleation is at the edge of IMC layer interface with the copper ribbon and the propagation is in

226 the shear direction; as the shear strength of the IMC layer material is lower than its tensile strength.

227   Based on the results of the study, presented in Figure 3 and Figure 4, a solder coating thickness of
228 between 20µm and 30µm is recommended as this will help to keep the crack growth rate low and also
229 keep the crack initiation temperature high; helping to increase the PV ribbon interconnection reliability.
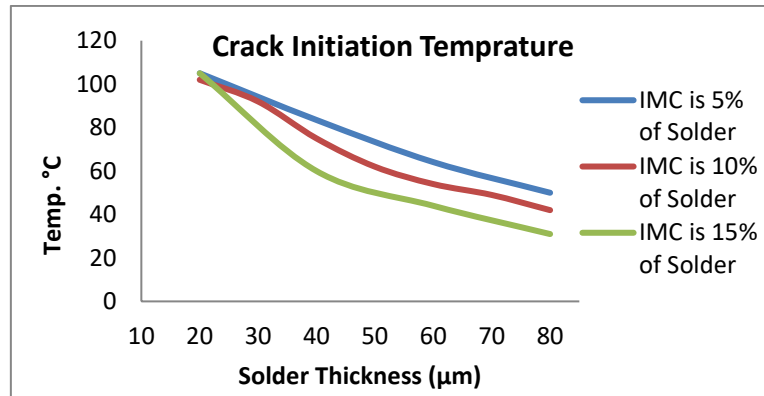
230

231   Figure 3 Effect of solder and IMC thickness on the crack initiation temperature (Silver thickness, copper
232   thickness and ribbon breadth are considered as 50µm, 200µm and 1mm, respectively)
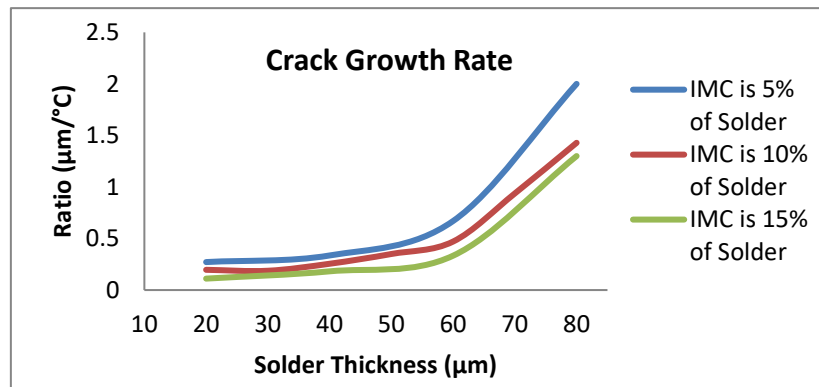
233
234   Figure 4 Effect of solder and IMC thickness on the crack growth rate (Silver thickness, copper thickness and
235   ribbon breadth are considered as 50µm, 200µm and 1mm, respectively)
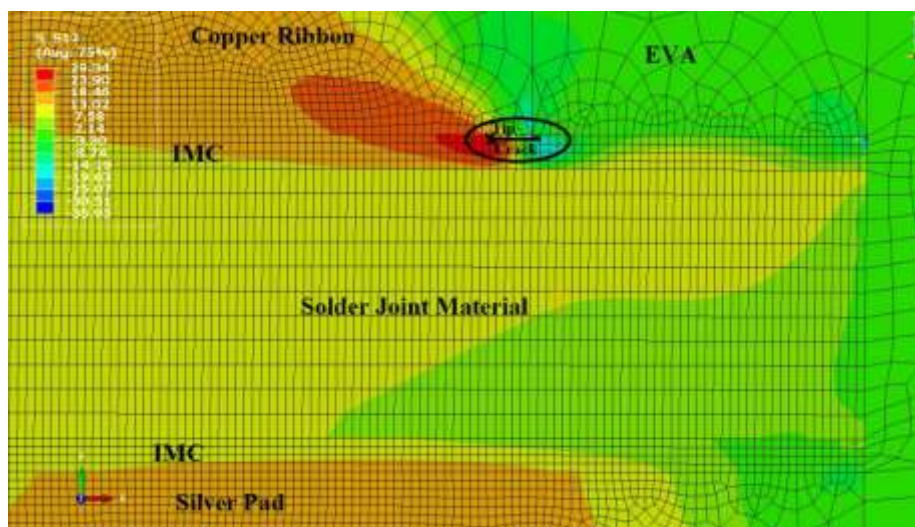
236

237   Figure 5 Crack's location and propagation direction in the IMC layer interface with the copper ribbon (Shear
238   stress distribution contour is displayed)

3.2 Effect of Ribbon Breadth Change

Figure 6 and Figure 7 show the effect of changing the ribbon width on the crack initiation temperature and crack growth rate, respectively, for different solder thicknesses. Our results presented in Figure 6 show that by increasing the ribbon width leads to an increase in the crack initiation temperature up to 1200µm; but for increases beyond the 1200µm limit the crack initiation temperature remains relatively constant. As will be noted from Figure 6, this trend is the same for all the solder coating thicknesses investigated in our study, although our results discussed earlier in Section 3.1 showed that increasing the solder coating thickness leads to a decrease in the crack initiation temperature. Our results presented in Figure 7 shows that the PV ribbon interconnections experienced a sharp increase in the crack growth rate beyond the 1200µm width limit. The reason for this sharp increase in crack growth rate is that the crack nucleation location has moved from the IMC layer interface with the copper ribbon (the IMC-Copper) to the IMC layer interface with the silver pad (the IMC-Silver pad). In addition, our results show that the crack locations in now nearer the centre of ribbon interconnect width, but the crack propagation is still in same shear direction. The location and direction of the initiated crack is in line with the experimental results from the literatures (Jeong, et al., 2012) and (Li, et al., 2009).

Based on the analysis of our results for both the crack initiation temperature and the crack growth rate for the ribbon interconnection geometries investigated, we will advise the use of ribbon interconnect widths of circa 1000µm, as this will lead to higher ribbon interconnection reliability for the PV module assembly. In addition, this recommendation will also lead to lower materials costs; as increasing the ribbon interconnection width leads to higher metallization and manufacturing costs. In addition to savings on metallization and materials costs, reducing the ribbon interconnection width helps to increase the PV solar module performance as the efficiency of the cell increases with the exposure of more silicon cell surface area to sun light.

Figure 6 Effect of ribbon breadth on the crack initiation temperature for different solder thicknesses (Silver thickness, copper thickness and IMC thickness are considered as 50µm, 200µm and 4µm, respectively)

267
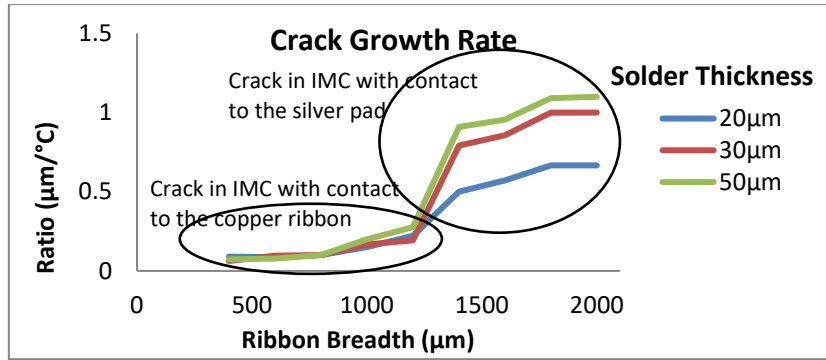
Figure 7 Effect of ribbon breadth on the crack growth rate for different solder thicknesses (Silver thickness,
copper thickness and IMC thickness are considered as 50µm, 200µm and 4µm, respectively)

3.3 Effect of Silver Thickness Change

The results of our study presented in Figure 8 and Figure 9 show effect of silver pad thickness on crack initiation temperature and the crack growth rate for the PV ribbon interconnection geometries investigated. The results show that crack initiation temperature and the crack growth rate decreases with increasing the silver pad thickness. However, Figure 8 suggests that the of crack initiation temperature for 20µm and 30µm solder coating thickness peaks at the silver pad thickness in range of 30µm to 50µm before decreasing. The results presented in Figure 9 shows that there is a significant change in the crack growth rate for silver pad thicknesses less than 50µm; as the crack nucleation is located in the IMC-Silver pad. Based on the results of the ribbon interconnection geometries investigated in our study, the recommended solder coating thickness will be 20µm, and we recommend silver pad thickness of between 40µm and 50µm which will help to achieve a higher ribbon interconnection reliability and lower material and manufacturing costs.

282
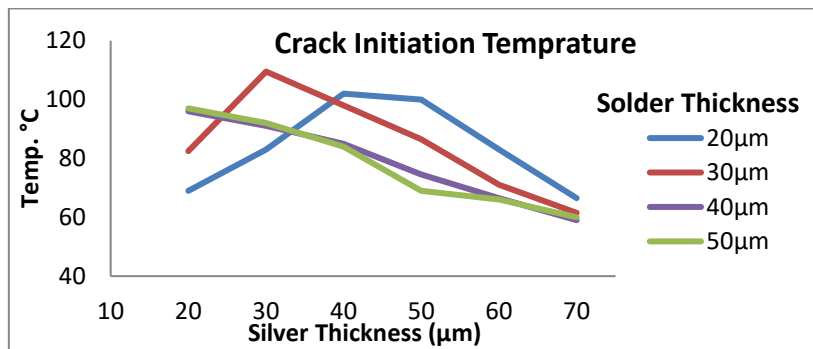
Figure 8 Effect of silver thickness on the crack initiation temperature for different solder thicknesses (Copper
thickness, ribbon breadth and IMC thickness are considered as 200µm, 1mm and 4µm, respectively)
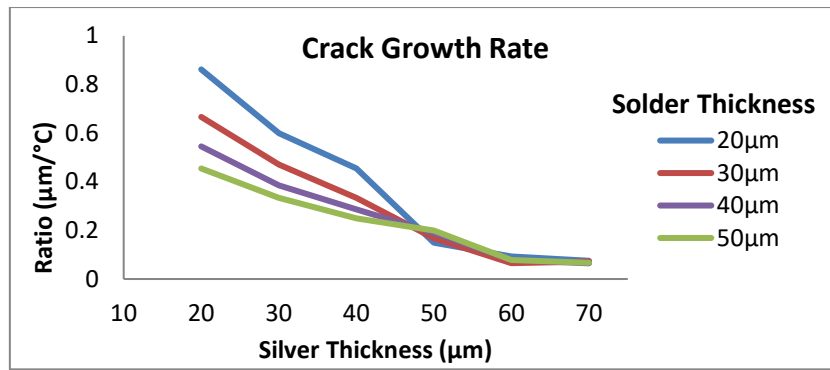
Figure 9 Effect of silver thickness on the crack growth rate for different solder thicknesses (Copper thickness, ribbon breadth and IMC thickness are considered as 200µm, 1mm and 4µm, respectively)

3.4 Effect of Copper Thickness Change

The results of our study presented in Figure 10 and Figure 11 show the effect of copper thickness on the crack initiation temperature and the crack growth rate for the PV ribbon interconnection geometries investigated. The results in Figure 10 show that increasing the copper thickness leads to a decrease in the crack initiation temperature; and that reduction in the crack initiation temperature is more pronounced for the thicker solder coatings. The results in Figure 11 also show that the lowest crack growth rate occurs at the 200µm copper thickness (the lowest point for all solder coating thicknesses). The results also show that the PV ribbon interconnection experiences high crack growth rates for the copper thickness below 200µm, due to crack location in the IMC Layer-Silver pad. The results also show that the PV ribbon interconnection experiences high crack growth rates for the copper thickness below 200µm, due to crack location in the IMC Layer-Silver pad. Hence, the 200µm copper thickness is recommended for PV ribbon interconnections as this gives the lowest crack propagation rate and better reliability.
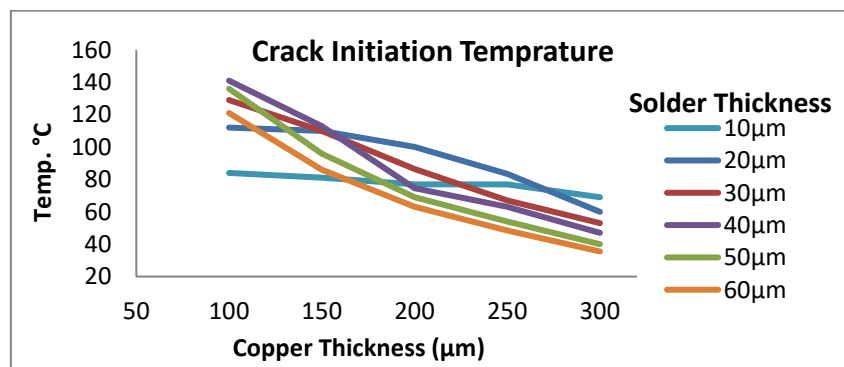
Figure 10 Effect of copper thickness on the crack initiation temperature for different solder thicknesses (Silver thickness, ribbon breadth and IMC thickness are considered as 50µm, 1mm and 4µm, respectively)

305
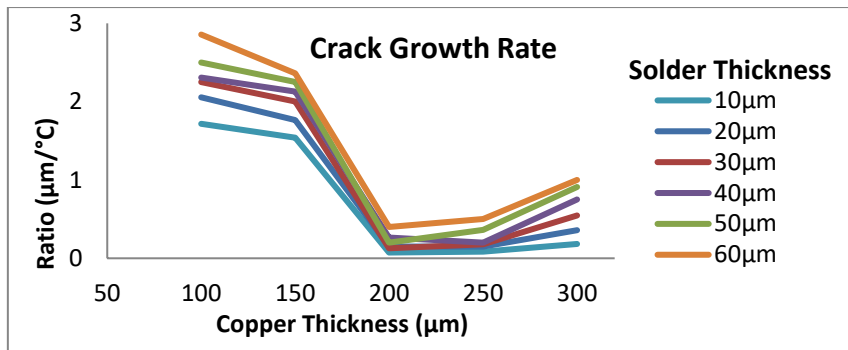
Figure 11 Effect of copper thickness on the crack growth rate for different solder thicknesses (Silver thickness, ribbon breadth and IMC thickness are considered as 50µm, 1mm and 4µm, respectively)

3.5 Interaction between Copper and silver Thickness Change

309
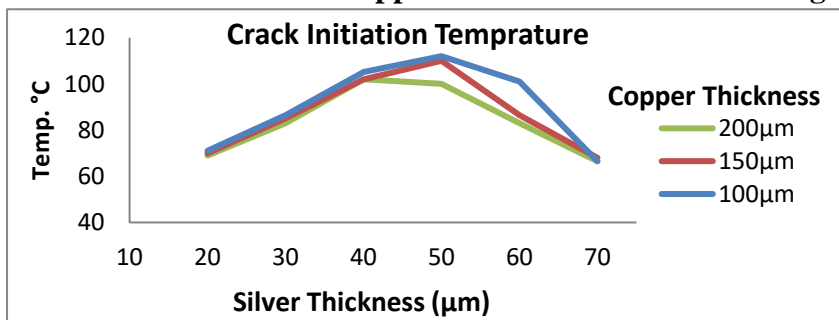
Figure 12 shows the plot of the effect of changing both silver pad and copper thickness on the crack initiation temperature for the PV ribbon interconnection geometries investigated in the study. This shows that reducing the copper thickness leads to an increase in the crack initiation temperature. The results also show that the silver pads with thickness between 40 µm to 50µm are recommended as this provides the higher crack initiation temperatures and hence better resistance to crack induces failures. Figure 13 shows the plot of the effect of changing the silver pad and copper thickness on the crack growth rates. The implication of the result in Figure 13 is that the crack growth rate for smaller silver pad thicknesses is significantly higher when compared with those for thicker silver pads. This is especially true for narrow copper ribbons, as in these cases the crack nucleated location is in the IMC-Silver pad.

320

321
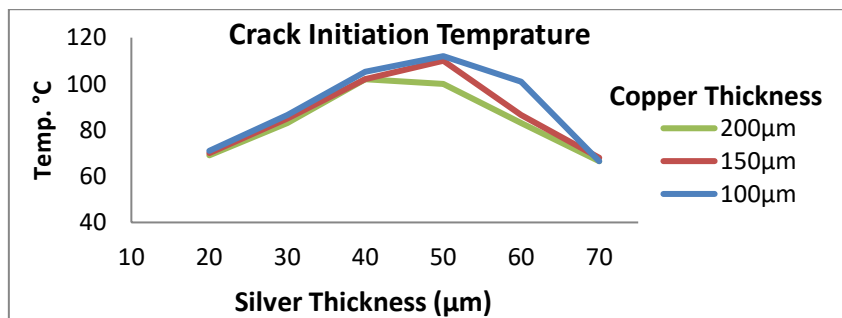
Figure 12 Effect of silver thickness on the crack initiation temperature for different copper thicknesses (Solder thickness, ribbon breadth and IMC thickness are considered as 20µm, 1mm and 4µm, respectively)
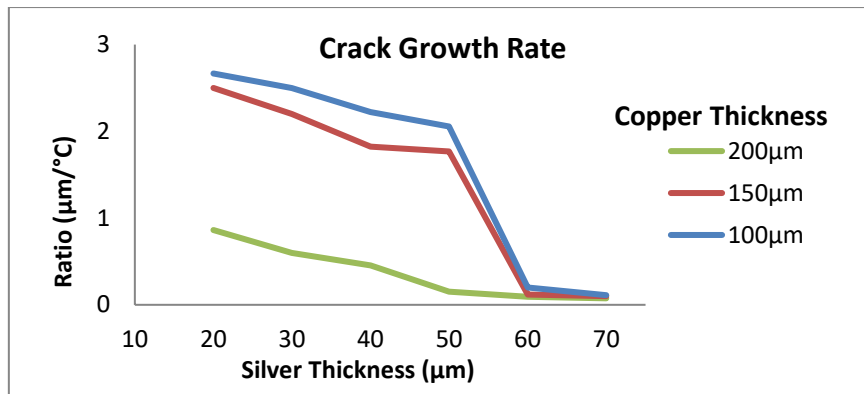
Figure 13 Effect of silver thickness on the crack growth rate for different copper thicknesses (Solder thickness, ribbon breadth and IMC thickness are considered as 20μm, 1mm and 4μm, respectively)

4. Conclusion

In this study, the Extended Finite Element Method (XFEM) in ABAQUS 2019 is employed to find the effect of geometrical dimensions of the PV module interconnection materials on the micro-crack initiation temperature and also the crack growth rate. The results show that PV module ribbon interconnection configuration has significant influence on the crack initiation temperature and the crack propagation rate; and consequently can adversely affect the PV module interconnection reliability. The results also show that micro-cracks are initiated at the edge of the IMC layer; and that cracks tend to propagate in shear direction and that crack growth rate is very dependent on the PV module ribbon interconnection geometry.

The main results of the study are summarised below:

- The crack nucleation is located in the IMC layer on the Silver pad side (the IMC-Silver pad) for ribbon interconnect configurations with copper wires widths greater than 1200μm, with copper wires thickness less than 200μm and with silver pads thickness less than 50μm. For other configurations the crack nucleation is located in the IMC layer on the Copper side (the IMC-Copper). When the crack nucleation location is in the IMC-Silver pad, the crack growth rate is significantly higher, which increases the crack related failures and adversely affects the reliability of the PV module interconnection.

- Increasing the ribbon interconnection solder coating thickness leads to an increase in the crack growth rate (for solder coatings greater than 50 μm thick) and also a decrease in the crack initiation temperature (circa linear relationship); and this reduction in crack initiation temperature is more pronounced for thicker IMCs when compared to thinner IMCs. For this reason, a solder coating thickness of between 20μm and 30μm is recommended as this will help to keep the crack growth rate low and also keep the crack initiation temperature high; helping to increase the PV ribbon interconnection reliability.

- Increasing the ribbon interconnection width leads to an increase in the crack initiation temperature for widths up to 1200μm; but the crack initiation temperature remains relatively constant for increases beyond the 1200μm limit. Based on the analysis of the results for both the crack initiation temperature and the crack growth rate for the ribbon

interconnection geometries investigated, we will advise the use of ribbon interconnect widths of circa 1000µm, as this will lead to higher ribbon interconnection reliability for the PV module assembly. In addition, this recommendation will also lead to lower materials costs; as increasing the ribbon interconnection width leads to higher metallization and manufacturing costs. In addition to savings on metallization and materials costs, reducing the ribbon interconnection width helps to increase the PV solar module performance as the efficiency of the cell increases with the exposure of more silicon cell surface area to sun light.

- The crack initiation temperature and the crack growth rate decreases with increasing Silver pad thickness (however, the crack initiation temperature for 20µm and 30µm solder coating thickness peaks at the silver pad thickness in range of 30µm to 50µm before decreasing). The recommended solder coating thickness for ribbon interconnections is 20µm, and we also recommend silver pad thickness of between 40µm and 50µm; which will help to achieve a higher ribbon interconnection reliability and lower material and manufacturing costs.

- Increasing the copper thickness leads to a decrease in the crack initiation temperature; and the reduction in the crack initiation temperature is more pronounced for thicker ribbon interconnection solder coatings. The lowest crack growth rate occurs at the 200µm copper thickness; hence the 200µm copper thickness is recommended for PV ribbon interconnections as this gives the lowest crack propagation rate and better reliability.

In summary, the results show that the crack initiation temperature and crack propagation rate are quite dependent on the dimensions of ribbon interconnection. For the different PV module ribbon interconnection configurations and design parameters investigated to establish the impact of interconnection geometry on the crack initiation temperature and crack propagation rate; a ribbon interconnection with 1000µm copper width, with 200µm copper thickness, with 50µm silver pad thickness and with 20µm solder thickness is recommended for low cost and high reliability PV solar ribbon interconnection.

The methodology developed can be used for investigating the thermal-fatigue life of PV module interconnections subjected to hot/cold service condition and for predicting the long term reliability of the PV solar module based on the knowledge of initial state (existing damage). The results of the study will be beneficial for researchers in predicting the propagation paths for existing micro-cracks during the thermal fatigue cycling under in-service PV module operating conditions; and hence for the predicting of PV Module interconnection reliability.

Acknowledgment

References

Li, J., Karppinen, J., Laurila, T. & Ka, J., 2009. Reliability of Lead-Free Solder Interconnections in Thermal and Power Cycling Tests. *IEEE Transactions on Components and Packaging Technologies, Vol. 32, No. 2.*

Li, J., Karppinen, J., Laurila, T. & Ka, J., 2012. Reliability of Lead-Free Solder Interconnections in Thermal and Power Cycling Tests. *IEEE Transactions on Components and Packaging Technologies, Vol. 32, No. 2.*

M. Sander, et al., 2011. Investigations on crack development and crack growth in embedded solar cells. *Reliability of Photovoltaic Cells, Modules, Components, and Systems.*

ABAQUS, I., 2017. *ABAQUS User's and Theory Manuals; Version 6.17,* s.l.: ABAQUS, Inc.: Providence Rhode Island, RI, USA.

AZoM, 2001. *Silver - Applications and Properties of Silver.* [Online]
Available at: https://www.azom.com/properties.aspx?ArticleID=600

AZoM, 2005. *Aluminium-Specifications, Properties, Classifications and Classes.* [Online]
Available at: https://www.azom.com/article.aspx?ArticleID=2863

Bidram, A., Davoudi, A. & Balog , R. S., 2012. Control and Circuit Techniques to Mitigate Partial Shading Effects in Photovoltaic Arrays. *IEEE Journal of Photovoltaics, Volume: 2 , Issue: 4,* pp. 532-546.

Cambridge University Engineering Department, 2003. *Materials Data Book.* Cambridge: Cambridge University Engineering Department Data Books.

Deng, X., Sidhu, R. j. & Chawla, N., 2005. Influence of reflow and thermal aging on the shear strength and fracture behavior of Sn-3.5Ag Solder/Cu joints. *Metallurgical and Materials Transactions A 36(1),* pp. 55-64.

DuPont™, 2014. *DuPont™ Tedlar® Polyvinyl Fluoride (PVF) Films.* [Online]
Available at: https://www.dupont.com/content/dam/dupont/products-and-services/membranes-and-films/pvf-films/documents/DEC_Tedlar_GeneralProperties.pdf

Eslami Majd, A. & Ekere, N. N., 2019. Numerical analysis on thermal crack initiation due to non-homogeneous solder coating on the round strip interconnection of photo-voltaic modules. *Solar Energy,* Volume 194, pp. 649-655.

Fei, H., Yazzie, K., Chawla, N. & Jiang, H., 2012. Modeling Fracture of Sn-Rich (Pb-Free) Solder Joints Under Mechanical Shock Conditions. *Journal of ELECTRONIC MATERIALS.*

Ferrara, C. & Philipp, D., 2012. *Why Do PV Modules Fail?.* Freiburg, Germany, s.n.

Fries, T.-P., 2018. *Extended Finite Element Methods (XFEM).* Berlin, Heidelberg: Encyclopedia of Continuum Mechanics. Springer.

427 H. Amalu, E. & N.N. Ekere, 2011. *Effects of inter-metallic compound on high temperature reliability of*
428 *flip chip interconnects for fine pitch applications.* s.l., s.n.

429 H. Amalu, E. & N.N. Ekere, 2016. Modelling evaluation of Garofalo-Arrhenius creep relation forlead-
430 free solder joints in surface mount electronic component assemblies. *Journal of Manufacturing*
431 *Systems.*

432 H. Lau, J., H. Pan, S. & Chang, . C., 2001. Nonlinear Fracture Mechanics Analysis of Wafer Level Chip
433 Scale Package Solder Joints with Cracks. *International Microelectronics And Packaging Society.*

434 Hasselbrink, E. et al., 2013. *Validation of the PVLife model using 3 million module-years of live site*
435 *data.* Tampa, FL, USA, IEEE 39th Photovoltaic Specialists Conference (PVSC).

436 Hermann, W., 2010. *How temperature cycling degrades photovoltaic-module performance,* s.l.: The
437 International Society for optics and photonics (SPIE), doi: 10.1117/2.1201007.003177.

438 IEA, 2019. *Renewables 2019, Paris.* [Online]
439 Available at: https://www.iea.org/reports/renewables-2019

440 Ishii, T. & Atsushi, M., 2017. Annual degradation rates of recent crystalline silicon photovoltaic
441 modules. *PROGRESS IN PHOTOVOLTAICS: RESEARCH AND APPLICATIONS.*

442 Itoh, U. et al., 2014. *Solder joint failure modes in the conventional crystalline Si module.* s.l., s.n.

443 Jeong, J.-S., Park, N. & Han, C., 2012. Field failure mechanism study of solder interconnection for
444 crystalline silicon photovoltaic module. *Microelectronics Reliability.*

445 Jiang, N., Clum, J. A., Chromik, R. R. & Cotts, E. J., 1997. Thermal Expansion of Several Sn-based
446 Intermetallic Compounds. *Scripta Materialia,Volume 37, Issue 12,* pp. 1851-1854.

447 Jing, X. et al., 2015. *Effect of pre-CMP annealing on TSV pumping in thermal budget and reliability*
448 *test.* Hsinchu, Taiwan, IEEE 22nd International Symposium on the Physical and Failure Analysis of
449 Integrated Circuits.

450 Lau, C.-S., Abdullah, M. Z., Mujeebu, M. A. & Yusop, N. M., 2014. Finite element analysis on the
451 effect of solder joint geometry for the reliability of ball grid array assembly with flexible and rigid
452 PCBs. *Journal of Engineering Science and Technology.*

453 Moës, N., Dolbow, J. & Belytschko, T., 1999. A finite element method for crack growth without
454 remeshing. *International Journal for Numerical Methods in Engineering,* pp. 131-150.

455 Mohammadi, S., 2008. *Extended Finite Element Method: For Fracture Analysis of Structures.*
456 s.l.:Wiley/Blackwell.

457 Owen-Bellini, M., Zhu, J., R. Betts, T. & Gottschalg, R., 2015. *Thermo-Mechanical Stresses of Silicon*
458 *Photovoltaic Modules.* Bangor, United Kingdom, s.n.

459 Pander, M., Schulze, S.-H. & Eber, . M., 2014. Mechanical modeling of electrically conductive
460 adhesives for photovoltaic applications. *29th European Photovoltaic Solar Energy Conference and*
461 *Exhibition.*

462 Pareek, S., Chaturvedi, . N. & Dahiya, R., 2017. Optimal interconnections to address partial shading
463 losses in solar photovoltaic arrays. *Solar Energy 155,* p. 537–551.

464 Sasi Kumar, T. et al., 2017. From cells to laminate: probing and modeling residual stress evolution in
465 thin silicon photovoltaic modules using synchrotron X-ray micro-diffraction experiments and finite
466 element simulations. *PROGRESS IN PHOTOVOLTAICS,* 25(RESEARCH AND APPLICATIONS), p. 791–
467 809.

468 Siviour, C. R., Walley, S., Proud, W. & Field, J., 2005. Mechanical properties of SnPb and lead-free
469 solders at high rates of strain. *Journal of Physics D: Applied Physics,* p. 4131–4139.

470 Taulaukian, Y., Kirby, R., Taylar, R. & Desai, P., 1975. *Thermal expansion Metallic Elements and*
471 *Alloys-Thermophysical Properties of Matter. Volume 12.* New York: SPRINGER SCIENCE+BUSINESS
472 MEDIA, LLC.

473 Tippabhotla, S. K. et al., 2017. From cells to laminate: probing and modeling residual stress evolution
474 in thin silicon photovoltaic modules using synchrotron X-ray micro-diffraction experiments and finite
475 element simulations: Probing and modeling residual stress evolution. *Progress in Photovoltaics*
476 *Research and Applications, 25,* p. 791–809.

477 Wang, H., Wang, A., Yang, H. & Huang, J., 2016. *Study on the Thermal Stress Distribution of*
478 *Crystalline Silicon Solar Cells In BIPV.* s.l., s.n., p. 429 – 435.

479 Zhong, W., Qin, F., An, T. & Wang, T., 2010. *Mechanical Properties of Intermetallic Compounds in*
480 *Solder Joints.* s.l., s.n.

481